Hindawi Publishing Corporation
The Scientific World Journal
Volume 2014, Article ID 869706, 9 pages
http://dx.doi.org/10.1155/2014/869706

Research Article

Photocatalytic Antibacterial Performance of Glass Fibers Thin Film Coated with N-Doped SnO_2/TiO_2

Peerawas Kongsong,[1] Lek Sikong,[1] Sutham Niyomwas,[2] and Vishnu Rachpech[1]

[1] *Department of Mining and Materials Engineering, Faculty of Engineering, Prince of Songkla University, Hat Yai, Songkhla 90112, Thailand*
[2] *Department of Mechanical Engineering, Faculty of Engineering, Prince of Songkla University, Hat Yai, Songkhla 90112, Thailand*

Correspondence should be addressed to Lek Sikong; lek.s@psu.ac.th

Received 19 August 2013; Accepted 30 October 2013; Published 12 February 2014

Academic Editors: C. He and G. Ouyang

Both N-doped and undoped thin films of $3SnO_2/TiO_2$ composite were prepared, by sol-gel and dip-coating methods, and then calcined at 600°C for 2 hours. The films were characterized by FTIR, XRD, UV-Vis, SEM, and XPS, and their photocatalytic activities to degrade methylene blue in solution were determined, expecting these activities to correlate with the inactivation of bacteria, which was confirmed. The doped and undoped films were tested for activities against Gram-negative *Escherichia coli* (*E. coli*) and *Salmonella typhi* (*S. typhi*), and Gram-positive *Staphylococcus aureus* (*S. aureus*). The effects of doping on these composite films included reduced energy band gap, high crystallinity of anatase phase, and small crystallite size as well as increased photocatalytic activity and water disinfection efficiency.

1. Introduction

The supply of safe drinking water is an issue of concern, particularly in developing countries. Although several initiatives have been successful in supplying safe drinking water to urban populations, the extent of these efforts still falls short of the required targets for sustainable development. In developing countries, water delivery systems are plagued by leakages, illegal connections, and vandalism, and precious water resources are mismanaged. In Africa, Asia, Latin America, and the Caribbean, nearly one billion people in rural areas have no access to sufficient clean water supplies [1]. Contaminated water commonly contains dangerous pathogens, and its consumption creates serious health effects and societal problems. In the past decade, many innovative disinfection technologies were developed and adopted as alternatives to chlorine and ozone associated disinfection processes, including germicide ultraviolet (UV) radiation and photocatalytic oxidation. The traditional disinfection approaches have potential risks, such as carcinogenic byproducts (DBPs). For the alternative technologies, diverse nanophotocatalysts such as titanium dioxide (TiO_2), zinc oxide (ZnO), cadmium sulfide (CdS), and silver nanoparticles have been widely studied and are considered promising due to their unique properties including large specific area and high reactivity [2].

TiO_2 is the most commonly used semiconductor photocatalyst and the most studied of the various nanomaterials. Activated by UV-A irradiation, its photocatalytic properties have been utilized in various environmental applications to remove contaminants from both water and air. A wealth of information on TiO_2 photocatalytic inactivation of bacteria has been acquired over the last 20 years. TiO_2 can kill both Gram-negative and Gram-positive bacteria, although Gram-positive bacteria are able to form spores and therefore are less sensitive. The exact bactericidal mechanism of reactive oxygen species (ROS) is not yet fully known, but the photocatalytic activity of TiO_2 produces them, and they are extremely reactive killing or deactivating microorganisms on contact [3].

There are many techniques to improve photoactivity such as control of phase morphology, crystallite size, and reducing band gap energy. Doping TiO_2 with N and combining it with SnO_2 could improve the photochemical activity [4, 5].

The aim of this work was to investigate the water disinfection efficiency of N-doped and undoped $3SnO_2/TiO_2$ composite films under UV radiation. The quantity of dopants in TiO_2 films was varied. The N-doped and undoped $3SnO_2/TiO_2$ composite films were formed as coatings on glass fibers, and the photocatalytic antibacterial effects of these films against Gram-negative *Escherichia coli* (*E. coli*), *Salmonella typhi* (*S. typhi*), and Gram-positive *Staphylococcus aureus* (*S. aureus*) were assessed. The fraction of viable bacteria that survived the treatment was determined with the spread plate technique. Furthermore, photocatalytic degradation of methylene blue dye in solution was also investigated, to correlate this activity with antibacterial activity.

2. Experimental

2.1. Materials and Methods. The TiO_2 composite films were formed on glass fibers (E-type) with two coating layers. The specific surface area of the starting glass fiber materials is $2\,m^2\,g^{-1}$ [6]. The first layer was $5SiO_2/TiO_2$, and this film was prepared by adding titanium (IV) isopropoxide (TTIP, 99.95%, Fluka Sigma-Aldrich) dropwise under vigorous stirring into a mixture solution containing ethanol (99.9%, Merck, Germany) and tetraethylorthosilicate (TEOS, 98%, Fluka Sigma-Aldrich). The second coating layer was (optionally N-doped) $3SnO_2/TiO_2$ composite. The N-doped $3SnO_2/TiO_2$ was prepared by mixing 10 mL glacial acetic, 0.289 g ammonium carbonate, and 0.315 g Tin (IV) chloride pentahydrate. For the first coating layer the concentration of SiO_2 was fixed at 5 mol%, while SnO_2 doped in the second layer was fixed at 3 mol%. Nitrogen at 20 mol% was used for doping of the $3SnO_2/TiO_2$ composite films, following Qin and coworkers [7]. The N-doped $3SnO_2/TiO_2$ solutions were stirred at room temperature for 60 min, and then 2 M HCl was added into the solution to adjust its pH to about 3.5.

The glass fibers were first kept at 500°C for 1 h in order to remove wax and then carefully cleaned with ethanol. A dip-coating apparatus was used to coat the fibers. The first coating with SiO_2/TiO_2 acted as a buffer layer on the glass fibers, and N-doped $3SnO_2/TiO_2$ sol was coated on the buffer layer as the second coating. A dipping speed of 1.0 mm/s into the sols gave homogeneous coatings. The coating films were turned into gels by drying at 60°C for 30 min. Then coated fibers were heated to 600°C at a heating rate of 10°C/min and held for 2 h. The coated glass fibers were cleaned by immersion in an ultrasonic bath of distilled water for 15 min in order to remove excess TiO_2 particles. The TiO_2 composite film coated glass fibers were dried at 105°C for 24 h. The samples were tested immediately after they had cooled in a desiccator to ambient temperature.

2.2. Material Characterization. Surface morphology was investigated by scanning electron microscopy (SEM) and energy-dispersive X-ray spectroscopy (EDS). XPS spectra were recorded with an AXIS Ultra DLD (Kratos Analytical Ltd., UK). Phase composition was characterized with an X-ray diffractometer (XRD) (Phillips E'pert MPD, Cu-Kα). The crystallite sizes were estimated from XRD peaks using the Scherrer equation [8]:

$$D = \frac{0.9\lambda}{\beta \cos\theta_\beta}, \quad (1)$$

where D is crystallite size, λ is the wavelength of X-ray radiation (Cu-Kα = 0.15406 nm), β is the angle width at half maximum height, and θ_β in degrees is the half diffraction angle of the peak centroid. The FTIR transmittance spectra of the samples were also analyzed in order to confirm hydroxyl functional groups (TiO_2–OH bonds) of the films. The band gap energies of TiO_2 and TiO_2 composites, in powder form, were measured by UV-Vis-NIR spectrometer with an integrating sphere attachment (Shimadzu ISR-3100 spectrophotometer) by using $BaSO_4$ as reference. The onset absorbances were determined by the linear extrapolation of the steep part of the UV absorption toward the base line.

2.3. Photocatalytic Reaction Test. The photocatalytic activities of TiO_2 and of N-doped $3SnO_2/TiO_2$ thin films on glass fibers were tested by observing the degradation of methylene blue (MB). The MB solution (50 mL) had 1×10^{-5} M initial concentration, and 1 g [8] of undoped or doped TiO_2 coated glass fibers were provided excitation from a 50 W UV-lamp (black light) in the 310–400 nm wavelength range, set at 32 cm distance from the samples. The photocatalytic reaction tests were done in a dark chamber, with various UV irradiation times up to 4 h. The remaining concentration of methylene blue was determined by UV-VIS spectrophotometer.

2.4. Photocatalytic Antibacterial Measurements. Gram-negative (*E. coli* and *S. typhi*) and Gram-positive (*S. aureus*) bacteria were obtained from the Microbiology Science Laboratory, Prince of Songkla University, Songkhla. The bacteria were grown aerobically in 4 mL of trypticase soy broth, at 37°C for 24 h. Then the bacterial solution was diluted in saline solution (0.85% NaCl) until the count of bacteria per milliliter of solution was in the range of 30–300. These counts were estimated by colony counter. The number of viable bacteria in a treated solution is readily quantified by spread plate technique, in which the sample is appropriately diluted and transferred to an agar plate. The grown colonies are counted, and each colony represents an initial viable bacterium in the plate culture. It is known that the initial bacterial concentration is an important factor affecting apparent antibacterial efficiency [9]. The initial bacterial concentration was set to about 10^3 CFU/mL. A 50 mL aliquot of bacterial suspension was treated with a 40 g/L dose of coated glass fibers, with exposure to UV irradiation for various durations. Then, 1 mL of treated suspension was sampled and cultured on MacConkey agar plates (*E. coli* and *S. typhi*) or Nutrient agar plates (*S. aureus*), by incubation at 37°C for 24 h. After incubation, the colony counts were recorded as estimates of viable bacteria counts.

To assess the antimicrobial mechanisms of the TiO_2 composite film coatings on glass fibers, the test fibers were dipped in 10^3 CFU/mL bacterial solution. After incubation, bacteria attached to the coatings were fixed with 0.05%

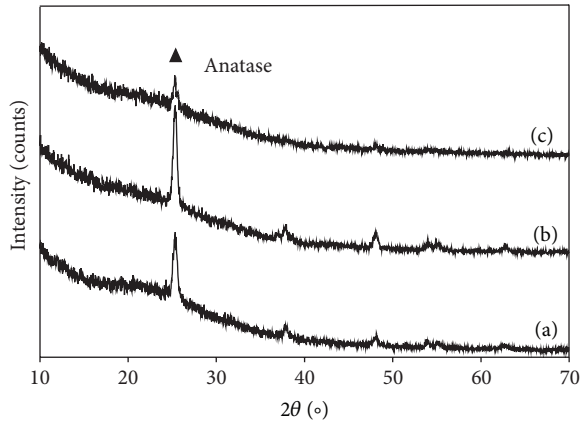

Figure 1: XRD patterns of TiO_2 thin films calcined at 600°C: (a) TiO_2, (b) $3SnO_2/TiO_2$, and (c) $20N/3SnO_2/TiO_2$.

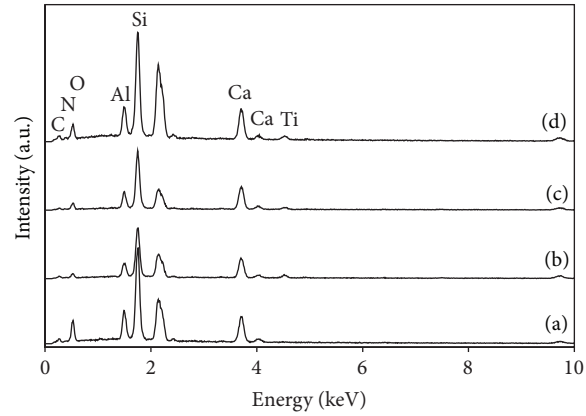

Figure 2: EDS spectra for (a) uncoated glass, (b) TiO_2, (c) $3SnO_2/TiO_2$ coating, and (d) $20N/3SnO_2/TiO_2$ coating, all calcined at 600°C.

Table 1: Effect of thin film type on its anatase crystallite size, energy band gap, and photocatalytic degradation of MB in 4 h.

Samples	Crystallite size (nm)	Energy band gap (eV)	% Degradation of MB in 4 h (%)
TiO_2	17.2	3.20	71.9
$3SnO_2/TiO_2$	17.2	3.20	80.3
$20N/3SnO_2/TiO_2$	9.8	3.03	89.5

glutaraldehyde in phosphate buffer saline and dehydrated sequentially by water-alcohol solutions (50%, 70%, 80%, 90%, and 100% alcohol, used in this order) for 30 min in each solution. After dehydrating by a series of ethanol solutions, specimens were dried in a critical-point dryer. The samples were mounted on stubs and coated with gold. The cell wall characteristics were observed by SEM imaging.

3. Results and Discussion

3.1. XRD Results of TiO_2 Thin Films. Figure 1 shows the XRD patterns of the thin films, namely, undoped $3SnO_2/TiO_2$ and $20N/3SnO_2/TiO_2$, after calcination at 600°C for 2 h. By comparison with anatase and rutile ASTM cards (American Society for Testing and Materials, cards JCPDS 21–1272 and JCPDS 21–1276), the films included anatase phase, and the various types of thin films did not differ in these observations. During the high calcinations temperature, TiO_2 had transformed from amorphous to anatase structure. The very broad diffraction peak at (1 0 1) plane ($2\theta = 25.3^\circ$) was due to the small crystallite size of TiO_2. The crystallite sizes calculated from Scherrer's equation are shown in Table 1. The calcined $20N/3SnO_2/TiO_2$ composite film had the smallest 9.8 nm crystallites. Nitrogen doping seems to hinder phase transformation from amorphous to anatase phase, leading to a low degree of crystallinity, while $3SnO_2/TiO_2$ had the highest degree of crystallinity (Figure 1). A tetragonal Bravais lattice type was evident, and the lattice constants were calculated from diffraction peaks ($a = b = 0.37821$ nm and $c = 0.95402$ nm for $3SnO_2/TiO_2$, and $a = b = 0.37852$ nm and $c = 0.96917$ nm for $20N/3SnO_2/TiO_2$). Compared with anatase TiO_2 ($a = b = 0.37852$ nm and $c = 0.95083$ nm), the lattice parameters a and b of $20N/3SnO_2/TiO_2$ were almost unchanged while c had increased. Therefore, the doping had slightly distorted the crystal lattice structure, as expected [10]. Both crystallite size and degree of crystallinity are known to affect photocatalytic activity.

3.2. EDS Spectra and Morphology of Surface Thin Films. The EDS spectra taken from TiO_2 and TiO_2 composite films are presented in Figure 2. The elements Si, Al, Ca, and O were mainly in the glass fiber substrates, while Ti, N, and O elements were in the composite films from TiO_2 and $20N/3SnO_2/TiO_2$. The peak for Sn is not observed, presumably because of its low dosage in the composite films. The morphologies of the coated surfaces are illustrated in Figure 3, as observed by SEM. The nucleation of anatase phase was homogeneous, and the film surface was smooth. However, some excess TiO_2 had remained randomly deposited on the coatings of glass fibers. Agglomeration of nanoparticles occurred in $3SnO_2/TiO_2$ films, but not in $20N/3SnO_2/TiO_2$ films. N-doping hindered anatase crystal growth, in agreement with the XRD spectra shown in Figure 1.

3.3. FTIR Analysis. The photogenerated hydroxyl groups on titanium dioxide surface can be characterized using FTIR transmittance spectra especially the peaks at 3200–3600 cm^{-1} [11, 12]. Figure 4 shows the FTIR spectra of TiO_2, $3SnO_2/TiO_2$, and $20N/3SnO_2/TiO_2$ calcined at 600°C. The bands appearing at about 3400–3468 cm^{-1} in TiO_2, $3SnO_2/TiO_2$, and $20N/3SnO_2/TiO_2$ coatings correspond to stretching vibrations of OH groups linked with titanium atoms (Ti–OH). This confirms that photocatalytic reactions took place on the sample surfaces. The broad and strong peaks at 1630–1640 cm^{-1} are ascribed to the bending vibration of OH groups, of free or absorbed water [13, 14]. The peaks at 1403 cm^{-1} in the spectrum of the $20N/3SnO_2/TiO_2$ sample are assigned to the vibrations of N–H bonds [15]. The peak

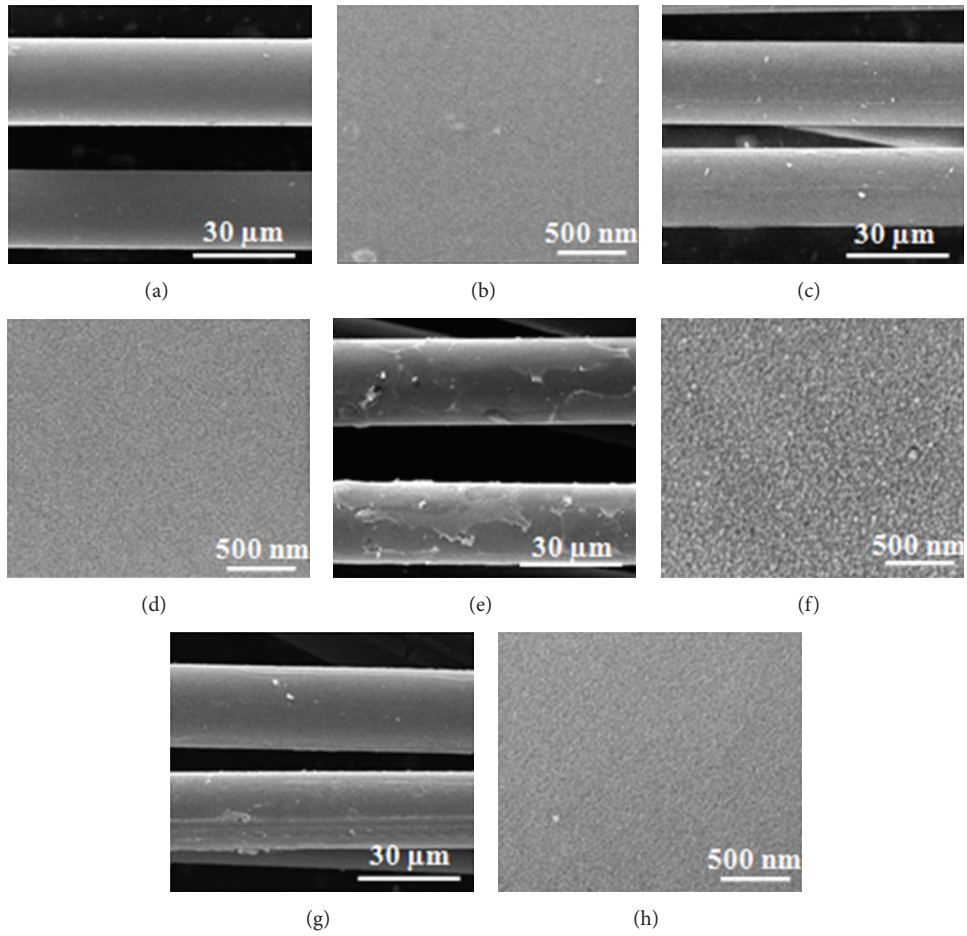

Figure 3: SEM images of glass fibers, some coated and calcined at 600°C: (a) uncoated 1,500x, (b) uncoated 60,000x, (c) TiO_2 1,500x, (d) TiO_2 60,000x, (e) $3SnO_2/TiO_2$ 1,500x, (f) $3SnO_2/TiO_2$ 60,000x, (g) $20N/3SnO_2/TiO_2$ 1,500x, and (h) $20N/3SnO_2/TiO_2$ 60,000x.

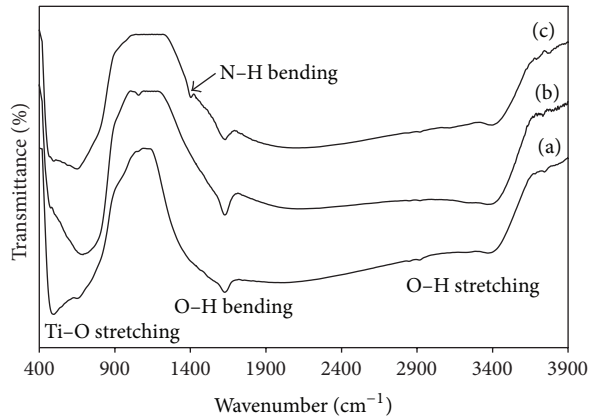

Figure 4: FTIR spectra of (a) pure TiO_2, (b) $3SnO_2/TiO_2$, and (c) $20N/3SnO_2/TiO_2$ powders calcined at 600°C.

at 600 cm^{-1} is ascribed to absorption bands of Ti–O and O–Ti–O, related to flexion vibration [16].

3.4. Energy Gap Measurement. The photon energy versus curve of pure TiO_2, $3SnO_2/TiO_2$, and $20N/3SnO_2/TiO_2$ are shown in Figure 5. The absorption edge energies were determined from the following relation:

$$E_g = \frac{1239.8}{\lambda}, \tag{2}$$

where E_g (eV) is the band gap energy of the sample and λ (nm) is the onset wavelength of the spectrum. The dopants affected the UV-Vis spectra by inhibiting recombination of electron-hole pairs, especially in the case of N-doping. The band gap energy of N-doped TiO_2 is shifted by 0.17 eV from the 3.20 eV of pure TiO_2 (Table 1), and $3SnO_2/TiO_2$ showed a smaller shift to 3.20 eV. These effects suggest a strategy for mediating photocatalysis through atomic-level doping of nanocatalysts. It can be seen that the absorption wavelength of $20N/3SnO_2/TiO_2$ photocatalyst is extended towards visible light ($\lambda = 409.2$ nm) relative to other varyingly doped samples [16] or pure TiO_2. The nitrogen doping hinders the growth of anatase phase (Figure 1) or it can reduce the crystallite size of TiO_2 composite films to be about 10 nm (Table 1), leading to a quantum confinement effect of nanocrystals and the highest photocatalytic activity.

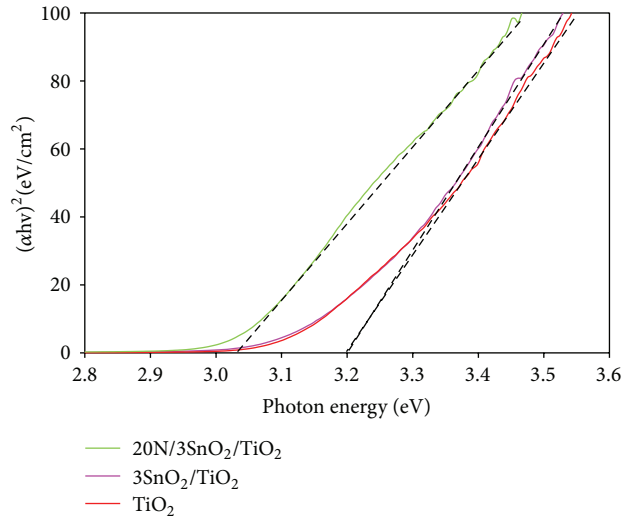

Figure 5: The photon energy versus $(\alpha hv)^2$ curve of representative pure TiO_2, $3SnO_2/TiO_2$, and $20N/3SnO_2/TiO_2$ samples calcined at 600°C.

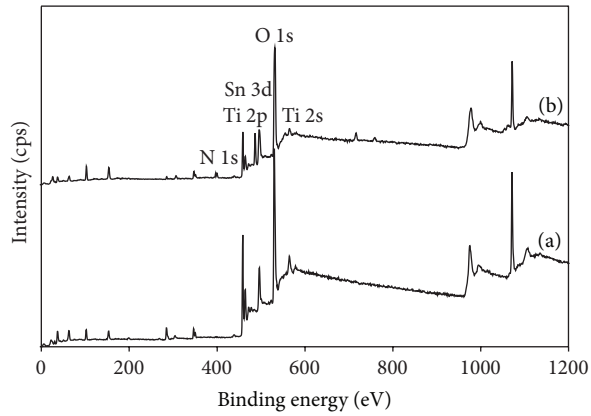

Figure 6: XPS spectra of (a) TiO_2 and (b) $20N/3SnO_2/TiO_2$ thin films, calcined at 600°C.

3.5. XPS Analysis. Figure 6 shows the X-ray photoelectron spectroscopic (XPS) spectra of TiO_2 and $20N/3SnO_2/TiO_2$ thin films. The Ti, O, N, and Sn elements were detected in $20N/3SnO_2/TiO_2$ thin films, in the respective percentages 7.25, 61.44, 1.35, and 2.39. The XPS peaks indicate that the codoped TiO_2 powders contain Ti, Sn, O, and N elements, and the binding energies of Ti 2p, Sn 3d, O 1s, and N 1s are 458, 486, 531, and 399 eV, respectively. The Sn 3d peak in the spectrum of Sn-TiO_{2-x}, shown in Figure 7, demonstrates tin on the surface of TiO_2. The 485.1 eV binding energy of tin in Sn-TiO_{2-x} is lower than the reference 486.6 eV energy reported for Sn 3d5/2-binding [17]. To assess the chemical state of N in $20N/3SnO_2/TiO_2$ thin films, a high-resolution XPS spectrum of N 1s was measured; see Figure 8. The N 1s binding energy peaks were broad and asymmetric, demonstrating at least two chemical states of N, with binding energies 397.0 and 399.6 eV. Each of these broad peaks was decomposed to three peaks, by curve fitting, indicating two

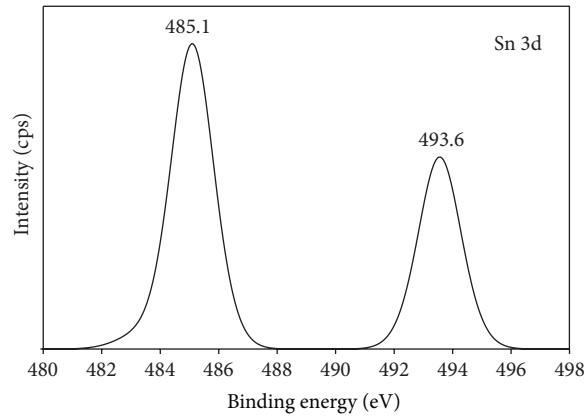

Figure 7: XPS spectrum of Sn 3d on the surface of $20N/3SnO_2/TiO_2$ thin film, calcined at 600°C.

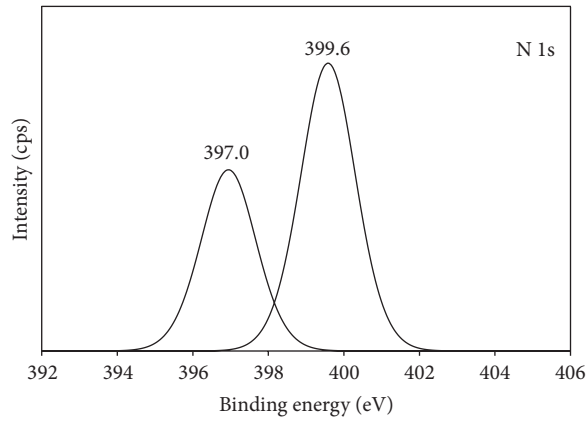

Figure 8: XPS spectrum of N 1s on the surface of $20N/3SnO_2/TiO_2$ thin film, calcined at 600°C.

different states of N. The main peak at 399.6 eV binding energy was attributed to the N–Ti–O environment, while the peaks at 397.0 eV were assigned to the substitutional nitrogen in the Ti–N structure [18].

3.6. Photocatalytic Activity Test. The photocatalytic activities of TiO_2 and the composite films were determined, by measuring degradation of methylene blue in solution (MB) with an initial concentration of 1×10^{-5} M, under UV for various irradiation times. Figure 9 shows the fraction of the MB remaining versus irradiation time, which equals current concentration relative to initial concentration, C/C_0. The $3SnO_2/TiO_2$ had better photocatalytic activity than pure TiO_2, possibly because photogenerated electrons can accumulate in SnO_2 and photogenerated holes in TiO_2, with a heterojunction formed at the SnO_2-TiO_2 interface. This would lower the recombination rate of photogenerated charge carriers, giving higher quantum efficiency and better photocatalytic activity [19]. The N-doped $20N/3SnO_2/TiO_2$ thin films had the most photoactivity (Figure 10). According to prior research, factors influencing the photoactivity of TiO_2 photocatalysts include crystalline phase, grain size,

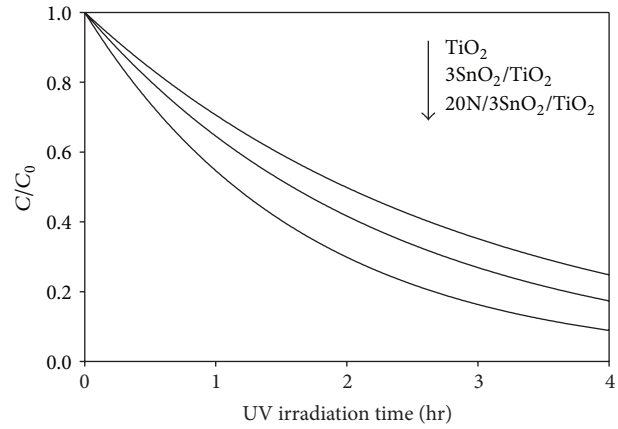

Figure 9: Photocatalytic degradation of MB in solution under UV excitation by various thin film coatings on glass fibers. The surface area of thin film available for reaction was held approximately constant, based on weight of glass fibers.

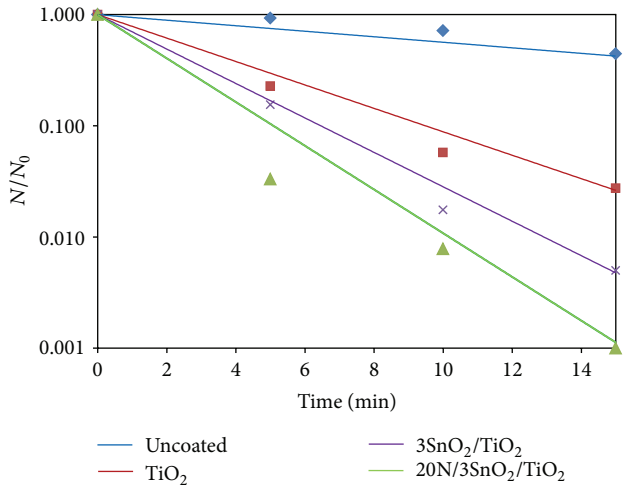

Figure 10: Antibacterial effects of coated glass fibers against *S. typhi* under UV irradiation.

specific surface area, surface morphology, and surface state (surface OH^- radicals), and these factors are correlated [20, 21]. Doping TiO_2 with N shifts its light absorption wavelength to the visible region, reduces crystallite size, and narrows its energy band gap (3.03 eV) [22]. A well-crystallized anatase phase facilitates transfer of photo-induced vacancies from bulk to surface, for degradation of organic composites, and effectively inhibits the recombination between photo-generated electrons and holes, giving excellent photocatalytic activity. As seen in Figure 1, the $20N/3SnO_2/TiO_2$ thin film had the smallest crystallite size, estimated to be about 9.8 nm (Table 1). The reaction rate constant k determined is a direct quantitative indicator of photocatalytic activity (Table 2), and k was highest at 0.6 hr^{-1} for the $20N/3SnO_2/TiO_2$ composite film, almost double that of pure TiO_2.

3.7. Photocatalytic Disinfection against Bacteria. The photo-inactivation of bacteria, in distilled water containing

Table 2: A summary of numerical fits of first-order kinetics to the degradation of MB.

Samples	Rate equation	Rate constant (k) (hr^{-1})	R^2
TiO_2	$C = e^{-0.34t}$	0.34	0.952
$3SnO_2/TiO_2$	$C = e^{-0.43t}$	0.43	0.975
$20N/3SnO_2/TiO_2$	$C = e^{-0.60t}$	0.60	0.974

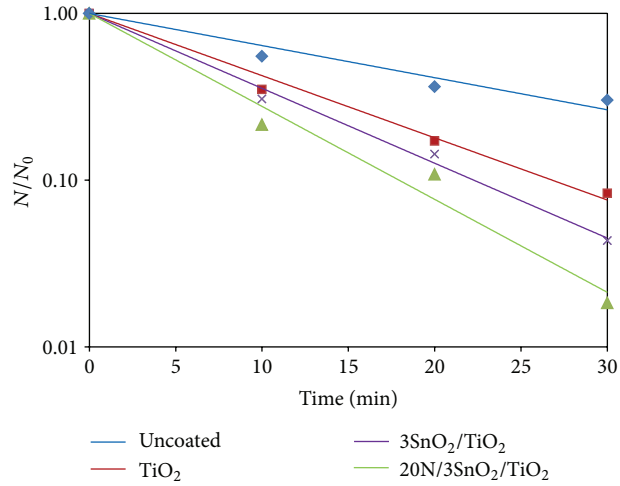

Figure 11: Antibacterial effects of glass fibers with various coatings against *E. coli* under UV irradiation.

the pathogen, was tested with UV excitation. The initial bacterial concentration was about 10^3 CFU/mL, and the results are shown in Figures 10–13. The survival rates of bacteria were estimated from CFU cultures that determine the number of viable cells. The survival curves in Figures 10–12 show the fraction surviving N/N_0, where N_0 is the initial and N the current viable count, at a given duration of irradiation. The $20N/3SnO_2/TiO_2$ film had the highest bactericidal activity, better than either pure TiO_2 or $3SnO_2/TiO_2$ with similar UV excitation, and dramatically better than UV alone. In the presence of $20N/3SnO_2/TiO_2$, *S. typhi* was almost completely inactivated within 10 min and completely killed within 15 min. In comparison with control fibers, TiO_2, and $3SnO_2/TiO_2$ thin films, *S. typhi* was killed 74%, 97%, and 99.5%, respectively, after 15 min UV irradiation (Figure 10). The results shown in Figure 11 for *E. coli* are qualitatively similar, with almost complete inactivation reached within 30 min and complete kill within 40 min in the best case, and the different film types had the same rank order as above. The rank order remained the same with *S. aureus*, which was completely killed within 60 min in the best case (Figure 12). Clearly the $20N/3SnO_2/TiO_2$ film had the best antibacterial effects against each pathogen tested. The antibacterial activity of the prepared films correlates well with the photocatalytic activity, determined from degradation of methylene blue. The inactivation rate constant, k of control (uncoated glass fibers under UV irradiation), TiO_2, $3SnO_2/TiO_2$, and $20N/3SnO_2/TiO_2$ films determined from Figures 10–12 illustrated in Table 3, is a

Table 3: A summary of numerical fits of first-order kinetics to the inactivation of bacteria.

Bacteria	Samples	Rate Equation	Rate constant (k) (min^{-1})	R^2
S. typhi	Uncoated	$N = e^{-0.050t}$	0.050	0.883
	TiO_2	$N = e^{-0.240t}$	0.240	0.975
	$3SnO_2/TiO_2$	$N = e^{-0.350t}$	0.350	0.990
	$20N/3SnO_2/TiO_2$	$N = e^{-0.450t}$	0.450	0.960
E. coli	Uncoated	$N = e^{-0.044t}$	0.044	0.935
	TiO_2	$N = e^{-0.086t}$	0.086	0.986
	$3SnO_2/TiO_2$	$N = e^{-0.103t}$	0.103	0.993
	$20N/3SnO_2/TiO_2$	$N = e^{-0.128t}$	0.128	0.975
S. aureus	Uncoated	$N = e^{-0.036t}$	0.036	0.888
	TiO_2	$N = e^{-0.058t}$	0.058	0.940
	$3SnO_2/TiO_2$	$N = e^{-0.070t}$	0.070	0.944
	$20N/3SnO_2/TiO_2$	$N = e^{-0.082t}$	0.082	0.936

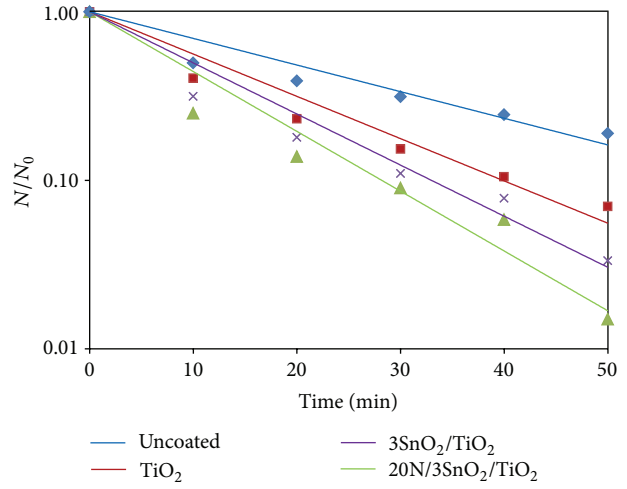

Figure 12: Antibacterial effects of glass fibers with various coatings against *S. aureus* under UV irradiation.

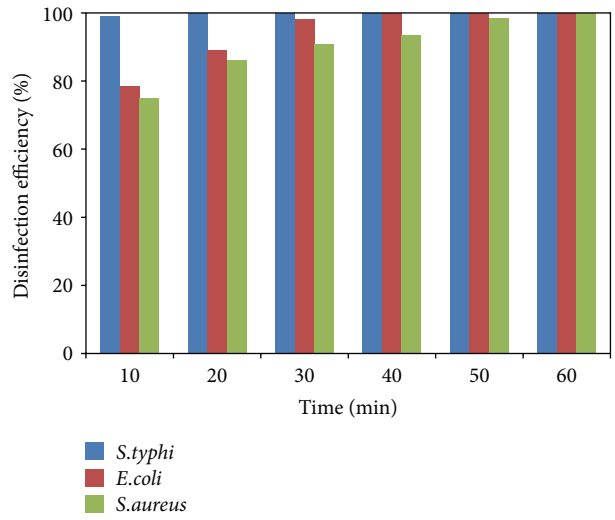

Figure 13: Antibacterial effects of $20N/3SnO_2/TiO_2$ coated glass fibers against *S. typhi*, *E. coli* and, *S. aureus* under UV irradiation.

direct quantitative indicator of antibacterial activity. It is seen that the k value of $20N/3SnO_2/TiO_2$ film was higher than that of other samples due to its smaller crystallite size or larger surface area. The killing rate, k, was the highest at 0.450 min^{-1} for *S. typhi* disinfection compared to 0.128 and 0.082 min^{-1} for *E. coli* and *S. aureus*, respectively. Figure 13 shows the antibacterial efficiency of $20N/3SnO_2/TiO_2$ composite thin film under UV irradiation. This thin film has a stronger antibacterial effect on Gram-negative than Gram-positive bacteria, because Gram-positive bacteria have thick cell walls composed of multilayered peptidoglycan [23], and also *E. coli* has thicker cell walls than *S. typhi*. The bactericidal effect of TiO_2 has been started from the damage of bacterial outer membranes after contact with reactive oxygen species (ROS), primarily hydroxyl radicals ($OH^{\bullet}$), which leads to phospholipid peroxidation and ultimately cell death. It has also been suggested that nanomaterials that can physically attach to a cell could be bactericidal on such contact [24].

The photos in Figure 14 show bacterial cultures on agar plates, illustrative of viable counts after various treatment times with $20N/3SnO_2/TiO_2$ under UV irradiation. The damage to cell walls of bacteria can be immediate on irradiation in the presence of TiO_2 thin films, and is followed by further damage to the cell membranes [25]. SEM images of bacteria before and after treatment with $20N/3SnO_2/TiO_2$ thin films are shown in Figures 15(a), 15(b), and 15(c) and Figures 15(d), 15(e), and 15(f), respectively. The cell walls of untreated bacteria were normal, and the number of germs was high (Figures 15(a)–15(c)). After 15 min of UV irradiation the cell walls and cell membranes were damaged by contact with TiO_2 composite films. The mechanism of this effect is that the photo-generated hydroxyl ($OH^{\bullet}$) and super oxygen ($O_2^{-\bullet}$) radicals react, as powerful oxidizing agents, with peptidoglycan (poly-*N*-acetylglucosamine and *N*-acetylmuramic acid) of bacterialcell wall [26].

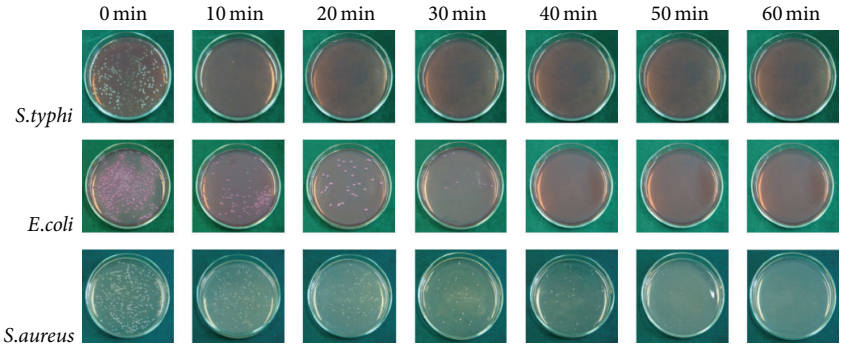

FIGURE 14: Growth of bacterial colonies on agar plates, after various treatment times. Glass fibers coated with 20N/3SnO_2/TiO_2 were used to treat *S. typhi, E. coli,* and *S. aureus* under UV irradiation, and the number of colonies corresponds to remaining viable count of bacteria.

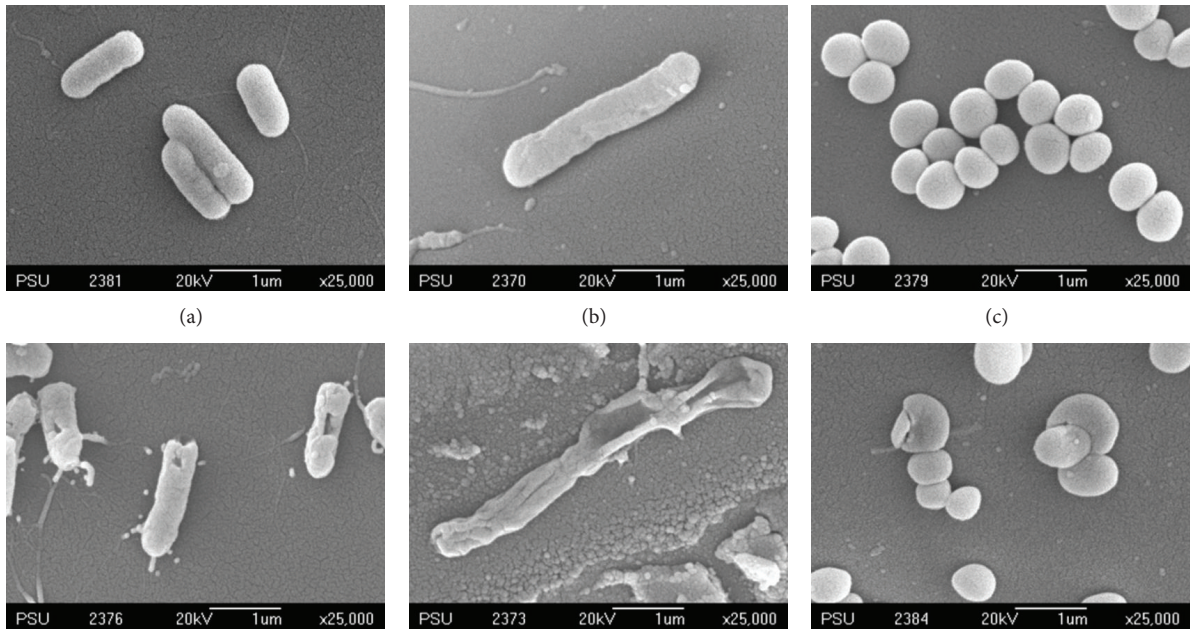

(a) (b) (c)

(d) (e) (f)

FIGURE 15: SEM images of bacteria observed on surface coated thin films: (a) untreated (*S. typhi*), (b) untreated (*E. coli*), (c) untreated (*S. aureus*), (d) irradiated for 15 min (*S. typhi*), (e) irradiated for 40 min (*E. coli*), and (f) irradiated for 60 min (*S. aureus*) of 20N/3SnO_2/TiO_2 composite thin films.

4. Conclusion

N-doped and undoped 3SnO_2/TiO_2 composite films were prepared as coatings on glass fibers, by sol-gel and dip-coating methods. The films were heated to 600°C at a rate of 10°C/min and held for 2 h, in order to form anatase phase. The 20N/3SnO_2/TiO_2 composite film had comparatively narrow band gap energy, high crystallinity of anatase phase, and small crystallite size as well as the highest photocatalytic activity of the films prepared. Its antibacterial activity under UV irradiation was superior to undoped TiO_2 films, correlating well with photocatalytic activity determined from MB degradation. Antibacterial activity was experimentally established against selected bacteria of both Gram-positive and Gram-negative types, with stronger antibacterial effects against Gram-negative type. The synthesized 20N/3SnO_2/TiO_2 film coated on glass fibers is antibacterial photocatalyst that will be suitable for water purification.

Conflict of Interests

The authors declare that there is no conflict of interests regarding the publication of this paper.

Acknowledgments

The authors gratefully acknowledge support by the Department of Mining and Materials Engineering, Faculty of Engineering, Prince of Songkla University and financial support

to Peerawas Kongsong and Lek Sikong by the Thailand Research Fund through the Royal Golden Jubilee Ph.D. Program (Grant no. PHD/0169/2553). Associate Professor Dr. Seppo Karrila, from the Faculty of Science and Technology, is also acknowledged for comments and suggestions, as is the copyediting service of the Research and Development Office of PSU.

References

[1] S. Gelover, L. A. Gómez, K. Reyes, and M. Teresa Leal, "A practical demonstration of water disinfection using TiO_2 films and sunlight," *Water Research*, vol. 40, no. 17, pp. 3274–3280, 2006.

[2] P. Gao, J. Liu, T. Zhang, D. D. Sun, and W. Ng, "Hierarchical TiO_2/CdS "spindle-like" composite with high photodegradation and antibacterial capability under visiblelight irradiation," *Journal of Hazardous Materials*, vol. 229-230, pp. 209–216, 2012.

[3] Q. Li, S. Mahendra, D. Y. Lyon et al., "Antimicrobial nanomaterials for water disinfection and microbial control: potential applications and implications," *Water Research*, vol. 42, no. 18, pp. 4591–4602, 2008.

[4] N. T. Nolan, D. W. Synnott, M. K. Seery, S. J. Hinder, A. Van Wassenhoven, and S. C. Pillai, "Effect of N-doping on the photocatalytic activity of sol-gel TiO_2 ," *Journal of Hazardous Materials*, vol. 211-212, pp. 88–94, 2012.

[5] L. C. Chen, F. R. Tsai, S. H. Fang, and Y. C. Ho, "Properties of sol-gel SnO_2/TiO_2 electrodes and their photoelectrocatalytic activities under UV and visible light illumination," *Electrochimica Acta*, vol. 54, no. 4, pp. 1304–1311, 2009.

[6] L. Kiwi-Minsker, I. Yuranov, B. Siebenhaar, and A. Renken, "Glass fiber catalysts for total oxidation of CO and hydrocarbons in waste gases," *Catalysis Today*, vol. 54, no. 1, pp. 39–46, 1999.

[7] H. L. Qin, G. B. Gu, and S. Liu, "Preparation of nitrogen-doped titania with visible-light activity and its application," *Comptes Rendus Chimie*, vol. 11, no. 1-2, pp. 95–100, 2008.

[8] Z. Liuxue, L. Peng, and S. Zhixing, "Photocatalysis anatase thin film coated PAN fibers prepared at low temperature," *Materials Chemistry and Physics*, vol. 98, no. 1, pp. 111–115, 2006.

[9] W. Zhang, Y. Chen, S. Yu, S. Chen, and Y. Yin, "Preparation and antibacterial behavior of Fe^{3+}-doped nanostructured TiO_2 thin films," *Thin Solid Films*, vol. 516, no. 15, pp. 4690–4694, 2008.

[10] Q. Ling, J. Sun, and Q. Zhou, "Preparation and characterization of visible-light-driven titania photocatalyst co-doped with boron and nitrogen," *Applied Surface Science*, vol. 254, no. 10, pp. 3236–3241, 2008.

[11] J. Xu, Y. Ao, D. Fu, and C. Yuan, "Synthesis of Bi_2O_3-TiO_2 composite film with high-photocatalytic activity under sunlight irradiation," *Applied Surface Science*, vol. 255, no. 5, pp. 2365–2369, 2008.

[12] K. Lv, H. Zuo, J. Sun et al., "(Bi, C and N) codoped TiO_2 nanoparticles," *Journal of Hazardous Materials*, vol. 161, no. 1, pp. 396–401, 2009.

[13] S. D. Sharma, D. Singh, K. K. Saini et al., "Sol-gel-derived superhydrophilic nickel doped TiO_2 film as active photo-catalyst," *Applied Catalysis A*, vol. 314, no. 1, pp. 40–46, 2006.

[14] Y. Li, G. Ma, S. Peng, G. Lu, and S. Li, "Boron and nitrogen codoped titania with enhanced visible-light photocatalytic activity for hydrogen evolution," *Applied Surface Science*, vol. 254, no. 21, pp. 6831–6836, 2008.

[15] X. Z. Bu, G. K. Zhang, Y. Y. Gao, and Y. Q. Yang, "Preparation and photocatalytic properties of visible light responsive N-doped TiO_2/rectorite composites," *Microporous and Mesoporous Materials*, vol. 136, no. 1–3, pp. 132–137, 2010.

[16] L. Sikong, M. Masae, K. Kooptarnond, W. Taweepreda, and F. Saito, "Improvement of hydrophilic property of rubber dipping former surface with Ni/B/TiO_2 nano-composite film," *Applied Surface Science*, vol. 258, no. 10, pp. 4436–4443, 2012.

[17] B. Xin, D. Ding, Y. Gao, X. Jin, H. Fu, and P. Wang, "Preparation of nanocrystalline Sn-TiO_2-X via a rapid and simple stannous chemical reducing route," *Applied Surface Science*, vol. 255, no. 11, pp. 5896–5901, 2009.

[18] L. Zhang, F. Lv, W. Zhang et al., "Photo degradation of methyl orange by attapulgite-SnO_2-TiO_2 nanocomposites," *Journal of Hazardous Materials*, vol. 171, no. 1–3, pp. 294–300, 2009.

[19] X. Cheng, X. Yu, Z. Xing, and J. Wan, "Enhanced photocatalytic activity of nitrogen doped TiO_2 anatase nano-particle under simulated sunlight irradiation," in *Proceedings of the International Conference on Future Energy, Environment, and Materials (FEEM '12)*, vol. 16, pp. 598–605, April 2012.

[20] A. J. Zaleska, J. W. Sobczak, E. Grabowska, and J. Hupka, "Preparation and photocatalytic activity of boron-modified TiO_2 under UV and visible light," *Applied Catalysis B*, vol. 78, no. 1-2, pp. 92–100, 2008.

[21] X. Zhang and Q. Liu, "Preparation and characterization of titania photocatalyst co-doped with boron, nickel, and cerium," *Materials Letters*, vol. 62, no. 17-18, pp. 2589–2592, 2008.

[22] J. Yang, H. Bai, Q. Jiang, and J. Lian, "Visible-light photocatalysis in nitrogen-carbon-doped TiO_2 films obtained by heating TiO_2 gel-film in an ionized N_2 gas," *Thin Solid Films*, vol. 516, no. 8, pp. 1736–1742, 2008.

[23] M. Ramani, S. Ponnusamy, and C. Muthamizhchelvan, "From zinc oxidenanoparticles to microflowers: a study of growth kinetics and biocidal activity," *Materials Science Engineering C*, vol. 32, no. 8, pp. 2381–2389, 2012.

[24] G. Rajakumara, A. Abdul Rahumana, S. Mohana Roopanb et al., "Fungus-mediatedbiosynthesis and characterization of TiO_2 nanoparticles and their activity againstpathogenic bacteria," *Spectrochimica Acta A*, vol. 91, pp. 23–29, 2012.

[25] X. Wang and W. Gong, "Bactericidal and photocatalytic activity of Fe^{3+}-TiO_2 thin films prepared by the sol-gel method," *Journal Wuhan University of Technology*, vol. 23, no. 2, pp. 155–158, 2008.

[26] L. Sikong, B. Kongreong, D. Kantachote, and W. Sutthisripok, "Inactivation of *Salmonella typhi* using Fe^{3+} doped TiO_2/3SnO_2 photocatalytic powders and films," *Journal of Nano Research*, vol. 12, pp. 89–97, 2010.